

Tribology of the lubricant quantized-sliding state

Ivano Eligio Castelli¹, Rosario Capozza², Andrea Vanossi^{3,2},
Giuseppe E. Santoro^{3,4}, Nicola Manini^{1,3}, and Erio Tosatti^{3,4}

¹*Dipartimento di Fisica and CNR-INFM, Università di Milano, Via Celoria 16, 20133 Milano, Italy*

²*CNR-INFM National Research Center S3 and Department of Physics,
University of Modena and Reggio Emilia, Via Campi 213/A, 41100 Modena, Italy*

³*International School for Advanced Studies (SISSA) and CNR-INFM Democritos
National Simulation Center, Via Beirut 2-4, I-34014 Trieste, Italy and*

⁴*International Centre for Theoretical Physics (ICTP), P.O.Box 586, I-34014 Trieste, Italy*

(Dated: December 4, 2018)

In the framework of Langevin dynamics, we demonstrate clear evidence of the peculiar quantized sliding state, previously found in a simple 1D boundary lubricated model [Phys. Rev. Lett. **97**, 056101 (2006)], for a substantially less idealized 2D description of a confined multi-layer solid lubricant under shear. This dynamical state, marked by a nontrivial “quantized” ratio of the averaged lubricant center-of-mass velocity to the externally imposed sliding speed, is recovered, and shown to be robust against the effects of thermal fluctuations, quenched disorder in the confining substrates, and over a wide range of loading forces. The lubricant softness, setting the width of the propagating solitonic structures, is found to play a major role in promoting in-registry commensurate regions beneficial to this quantized sliding. By evaluating the force instantaneously exerted on the top plate, we find that this quantized sliding represents a dynamical “pinned” state, characterized by significantly low values of the kinetic friction. While the quantized sliding occurs due to solitons being driven gently, the transition to ordinary unpinned sliding regimes can involve lubricant melting due to large shear-induced Joule heating, for example at large speed.

PACS numbers: 68.35.Af, 05.45.Yv, 62.20.Qp, 81.40.Pq, 46.55.+d

I. INTRODUCTION

When a confined lubricant is characterized by a large surface-to-volume ratio, the surface features of the confining walls may strongly affect its tribological properties. If the width of the lubricant film is reduced to a few atomic layers, as in the boundary-sliding regime, the atoms in the film tend generally to be ordered into layers parallel to the bounding substrates.^{1,2} Both numerical simulations and experiments generally conclude that, in such a strongly confined geometry, the film behaves like a solid, even at temperatures significantly higher than its bulk melting temperature.³ In real operative conditions, moreover, the case of “dry” friction is quite exceptional. A physical contact between two solids is generally mediated by so-called “third bodies”, which act like a lubricant film.⁴ For crystals sliding on crystals, one may consider the moving contact as characterized schematically by three inherent length scales: the periods of the bottom and top substrates, and the period of the embedded lubricant structure.

The problem of boundary lubricated friction is fascinating both from the fundamental point of view and for applications. Interesting dynamical behaviors, with possible tribologically important implications of an irregular distribution of the lubricant velocity in between the sliding surfaces, have recently been observed in numerical simulations, depending on the “degree” of geometrical incommensurability defining the moving interface.^{5–8} The prominent nontrivial feature of those simulation is an asymmetry in the relative sliding velocity of the intermediate lubricating sheet relative to the two sub-

strates. Strikingly, this velocity asymmetry takes an exactly quantized value which is uniquely determined by the incommensurability ratios and is insensitive to all other physical parameters of the model. The occurrence of this surprising and robust regime of motion, giving rise to perfectly flat plateaus in the ratio of the time-averaged lubricant center-of-mass (CM) velocity to the externally imposed relative speed, was ascribed to the intrinsic topological nature of this quantized dynamics. The phenomenon, investigated in detail in a rather idealized 1D geometry,^{9–14} was explained by the corrugation of a sliding confining wall rigidly dragging the topological solitons (kinks or antikinks) that the embedded lubricant structure forms with the other substrate. Evidence of the existence of this peculiar regime of motion was then confirmed shortly after for a substantially less idealized 2D model of boundary lubrication, where atoms were allowed to move perpendicularly to the sliding direction and interacted via LJ potentials¹⁵. The solitonic transverse corrugations of the lubricant, propagating inside the film from bottom to top, were observed to favor the kink (or antikink) tendency to pin to the top-layer spatial periodicity, thus strengthening the quantization mechanism.

In this work, we investigate the tribological signature of the quantized-velocity state for such a 2D multi-layer solid lubricant under shear. Its robustness against thermal effects (implemented by means of a standard Langevin approach), quenched disorder in the confining substrates, and over a wide range of loading forces is analyzed in detail. The lubricant softness, setting the width of the propagating solitonic structures, together with the

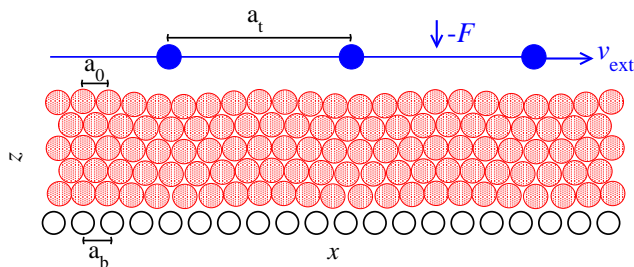


FIG. 1: (color online). A sketch of the model with the rigid top (solid circles) and bottom (open) crystalline sliders (of lattice spacing a_t and a_b respectively), the former moving at externally imposed x -velocity v_{ext} . One or more solid lubricant layers (shaded) of rest equilibrium spacing a_0 are confined in between.

soliton coverage number, is considered in promoting inregistry commensurate regions beneficial to the quantized sliding. Hysteretic termination and kinetic friction are properly evaluated to highlight tribological differences with respect to ordinary unpinned sliding regimes.

The paper is organized as follows. In Sec. II, we summarize the main features of the 2D-implemented tribological confined model, together with the numerical procedure adopted to solve the system of coupled equations describing the dissipative particle dynamics and top plate motion at finite temperatures. Section III is devoted to prove the robustness of the quantized dynamical regime against many physical parameters of the model. In Sec. IV the relative lubricant-lubricant and lubricant-substrate interactions are varied to study the role of the confined film softness. By evaluating the force instantaneously exerted on the advancing plate in Sec. V, we characterize the tribological features of the quantized dynamics and show that it corresponds to significantly low kinetic friction force. The transition towards ordinary sliding regimes can involve lubricant melting due to large shear-induced Joule heating, leading to a higher-friction sliding state. As detailed in Sec. VI, within the framework of our rigid, constant-speed driving, we observe an intermittent stick-slip dynamics, associated to tiny amplitude fluctuations, in the kinetic friction force experienced by the top substrate while in the quantized-velocity state. Discussions and conclusions are given in Sec. VII.

II. THE 2D CONFINED LUBRICATED MODEL

Our system is composed of two rigid walls made of equally-spaced atoms and N_l identical lubricant atoms confined in between, organized in N_{layer} layers, see Fig. 1 where $N_{\text{layer}} = 5$. The lubricant atoms move under the action of pairwise Lennard-Jones (LJ) potentials

$$\Phi_a(r) = \epsilon_a \left[\left(\frac{\sigma_a}{r} \right)^{12} - 2 \left(\frac{\sigma_a}{r} \right)^6 \right] \quad (1)$$

describing the reciprocal interactions. The cutoff radius is set at $r = r_c = 2.49 \sigma_a$, where $\Phi_a(r_c) \simeq -8.4 \cdot 10^{-3} \epsilon_a$.

For the two substrates and the lubricant we assume three different kinds of atoms, and characterize their mutual interactions (Φ_{bl} , Φ_{ll} and Φ_{tl} refer to potential energies for the bottom-lubricant, lubricant-lubricant, and top-lubricant interactions, respectively) with the following LJ radii σ_a

$$\sigma_{tl} = a_t, \quad \sigma_{bl} = a_b, \quad \text{and} \quad \sigma_{ll} = a_0, \quad (2)$$

which, for simplicity, are set to coincide with the fixed spacings a_t and a_b between neighboring substrate atoms, and the average x -separation a_0 of two neighboring lubricant atoms, respectively. This restriction is only a matter of convenience, and is not essential to the physics we are describing. These three different periodicities a_t , a_0 and a_b define two independent ratios:

$$\lambda_t = \frac{a_t}{a_0}, \quad \lambda_b = \frac{a_b}{a_0}, \quad (3)$$

the latter of which we take closer to unity, $\max(\lambda_b, \lambda_b^{-1}) < \lambda_t$, so that the lubricant is less off-register to the bottom substrate than to the top.

For simplicity, we fix the same LJ interaction energy $\epsilon_{tl} = \epsilon_{ll} = \epsilon_{bl} = \epsilon$ for all pairwise coupling terms and the same mass m of all particles. We take ϵ , a_0 , and m as energy, length, and mass units. This choice defines a set of “natural” model units for all physical quantities: for instance velocities are measured in units of $\epsilon^{1/2} m^{-1/2}$. In the following, all mechanical quantities are expressed implicitly in the respective model units.

The interaction with the other lubricant and sliders’ particles produces a total force acting on the j -th lubricant particle, of coordinate \vec{r}_j , given by

$$\vec{F}_j = -\frac{\partial}{\partial \vec{r}_j} \left[\sum_{i=1}^{N_t} \Phi_{tl}(|\vec{r}_j - \vec{r}_{ti}|) + \sum_{\substack{j'=1 \\ j' \neq j}}^{N_l} \Phi_{ll}(|\vec{r}_j - \vec{r}_{j'}|) + \sum_{i=1}^{N_b} \Phi_{bl}(|\vec{r}_j - \vec{r}_{bi}|) \right], \quad (4)$$

where \vec{r}_{ti} and \vec{r}_{bi} are the positions of the N_t top and N_b bottom atoms. By convention, we select the frame of reference where the bottom layer is static, with the atoms located at

$$r_{bi x}(t) = i a_b, \quad r_{bi z}(t) = 0. \quad (5)$$

The top slider is rigidly driven at a constant horizontal velocity v_{ext} , and can also move vertically (its inertia equals the total mass $N_t m$ of its atoms) under the action of the external loading force F applied to each particle in that layer and that due to the interaction with the particles in the lubricant layer:

$$r_{ti x}(t) = i a_t + v_{ext} t, \quad r_{ti z}(t) = r_{ti z}(t), \quad (6)$$

where the equation governing r_{tz} is

$$N_t m \ddot{r}_{tz} = - \sum_{i'=1}^{N_t} \sum_{j=1}^{N_l} \frac{\partial \Phi_{t1}}{\partial r_{t i' z}} (|\vec{r}_{t i'} - \vec{r}_j|) - N_t F. \quad (7)$$

To remove the Joule heat, and control the lubricant temperature in this driven system, rather than a Nosé-Hoover thermostat^{16,17} as in Ref. 15, we use a standard implementation of the Langevin dynamics,¹⁸ with the addition of a damping term plus a Gaussian random force $\vec{f}_j(t)$ to the Newton equations for the lubricant particles. The damping force includes the contributions of the energy dissipation into both individual substrates:

$$\vec{f}_{\text{damp } i} = -\eta \dot{\vec{r}}_i - \eta (\dot{\vec{r}}_i - \dot{\vec{r}}_t). \quad (8)$$

Taking into account this double contribution to the η -dissipation, the Gaussian null-average random forces satisfy the relation

$$\langle f_{jx}(t) f_{jx}(t') \rangle = 4\eta k_B T \delta(t - t') \quad (9)$$

and similarly for the \hat{z} components, such that in a static configuration ($v_{\text{ext}} = 0$) the Langevin thermostat leads to a steady state characterized by standard Boltzmann equilibrium

$$\langle E_k \rangle = 2 N_l \frac{1}{2} k_B T, \quad (10)$$

with the total kinetic energy of the lubricant $E_k = \frac{1}{2} \sum_i m \dot{\vec{r}}_i^2$. This algorithm represents a simple but numerically stable and effective phenomenological approach to describe energy dissipation into the substrates occurring through the excitation of phonons and (in the case of metals) of electron-hole pairs. As we shall see below, the Langevin thermostat controls and compensates reasonably well the expected Joule heating of the substrate, even in the sliding regime ($v_{\text{ext}} \neq 0$).

We adopt a fairly small value $\eta = 0.1$ leading to underdamped lubricant dynamics. To guarantee a detailed force balance (Newton's third law), we add the following force term

$$\eta \sum_i^{N_l} (\dot{\vec{r}}_i - \dot{\vec{r}}_t) = \eta N_l (\vec{v}_{\text{cm}} - \dot{\vec{r}}_t) \quad (11)$$

to the equations for the motion of the top layer. While the \hat{z} -component of this additional term has a real influence on the motion governed by Eq. (7), of course its \hat{x} -component only affects the external force F_k required to maintain the velocity component \dot{r}_{tx} constant and equal to v_{ext} .

We integrate the ensuing equations of motion within a x -periodic box of size $L = N_l a_0$, by means of a standard fourth-order Runge-Kutta method.¹⁹ We usually start off the dynamics of a single lubricant layer from equally-spaced lubricant particles at height $r_{iz} = a_b$ and with the

top layer at height $r_{tz} = a_b + a_t$, but we consider also different initial conditions. For several layers, we initialize the system with lubricant particles at perfect triangular lattice sites, and the top slider correspondingly raised. After an initial transient, sometimes extending for several hundred time units, the sliding system reaches its dynamical steady state. In the numerical simulations, an adiabatic variation of the external driving velocity (a controllable parameter in tribological experiments) is considered and realized by changing v_{ext} in small steps $\delta v = 0.1$, letting the system evolve at each step for a time long enough for all transient stresses to relax, in practice 1500 time units. In the calculations presented below, we compute accurate time-averages of the physical quantities of interest by averaging over a simulation time of 3000 time units or more after the transient is over. At higher temperature, fluctuations of all physical quantities around their mean values increase, sometimes requiring even longer simulation times to obtain well-converged averages. To estimate error bars of all average quantities, we split the whole trajectory into 30 pieces of equal duration, and then evaluate the standard deviation of the averages carried out over each individual interval.

III. THE ROBUSTNESS OF THE PLATEAU DYNAMICS

Here we prove the robustness of the quantized velocity plateau dynamics against thermal fluctuations, changes in vertical load and the effect of quenched disorder in the confining substrates. In our simulations, we take into account complete layers, realizing an essentially crystalline lubricant configuration at the given temperature, generally kept below its melting temperature. To investigate the dragging of kinks and the ensuing exact velocity-quantization phenomenon, we evaluate the ratio $w = \overline{v_{\text{cm } x}}/v_{\text{ext}}$ of the time-averaged lubricant CM sliding velocity to the externally imposed sliding speed v_{ext} stays pinned to an exact geometrically determined plateau value, while v_{ext} itself or temperature T or even relative substrate corrugation amplitudes are made vary over wide ranges. In detail, the plateau velocity ratio

$$w_{\text{plat}} = \frac{\overline{v_{\text{cm } x}}}{v_{\text{ext}}} = \frac{\frac{1}{a_0} - \frac{1}{a_b}}{\frac{1}{a_0}} = \frac{\lambda_b - 1}{\lambda_b} = 1 - \frac{1}{\lambda_b} \quad (12)$$

is a function uniquely determined by the excess linear density of lubricant atoms with respect to that of the bottom substrate, thus of the length ratio λ_b , Eq. (3). Despite not affecting the w_{plat} value, the top length ratio λ_t also plays an important role, since it sets the kink coverage $\Theta = N_{\text{kink}}/N_t = (1 - \lambda_b^{-1}) \lambda_t$: assuming that the 1D mapping to the FK model sketched in Ref. 7 makes sense also in the present richer 2D geometry, the coverage ratio Θ should affect the pinning strength of kinks to the top corrugation, thus the robustness of the velocity plateau, as we will show in Sec. IV below.

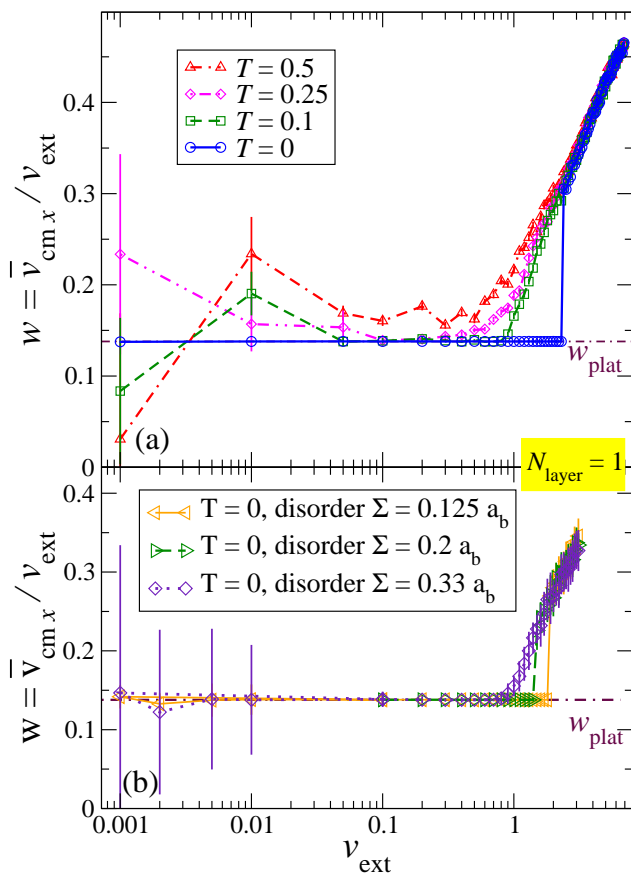


FIG. 2: (color online). The time-averaged velocity ratio $w = \overline{v_{\text{cm},x}}/v_{\text{ext}}$ of a single lubricant layer as a function of the adiabatically increased top-slider velocity v_{ext} for different temperatures of the Langevin thermostat (panel (a)) and for distinct degrees of quenched disorder in the bottom substrate (panel (b)); atomic random displacements are taken in a uniform distribution in the interval $[-\Sigma/2, \Sigma/2]$ horizontally and $[-\Sigma/4, \Sigma/4]$ vertically away from the ideal positions of Eq. (5). All simulations are carried out with a model composed by 4, 29 and 25 atoms in the top lubricant and bottom layers respectively, with an applied load $F = 25$. The plateau velocity ratio (dot-dashed line) is $w_{\text{plat}} = \frac{4}{29} \simeq 0.138$, Eq. (12).

As a convenient system for practical calculations we consider a bottom substrate made of 25 particles, and 29 lubricant particles in each layer, i.e. $\lambda_b = 29/25 = 1.16$, which produces 4 kinks every 29 lubricant particles in each layer. This value of λ_b is not to be considered in any way special: we found perfect plateau sliding for many other values of λ_b . Moreover we also investigated the plateau dynamics for an anti-kink configuration $\lambda_b = 21/25 = 0.84$.

Figure 2(a) reports the time-averaged horizontal velocity $\overline{v_{\text{cm},x}}$ of the single-layer lubricant CM, as a function of the velocity v_{ext} of a fully commensurate top layer ($\Theta = 1$) for several temperatures set by the Langevin thermostat. The velocity ratio $w = \overline{v_{\text{cm},x}}/v_{\text{ext}}$ is generally a nontrivial function of v_{ext} , that for low temperature

(here $T = 0$ and $T = 0.1$) displays a wide flat plateau followed by a regime of continuous evolution. The plateau extends over a wide range of external driving velocities, up to a critical depinning velocity v_{crit} , whose precise value is obtained by ramping v_{ext} “adiabatically”. Beyond v_{crit} , the lubricant leaves the plateau speed and, at finite temperature, moves up toward the symmetrical speed $w = 0.5$, as dictated by the thermostat dissipation. At zero temperature, the plateau state is abandoned with a discontinuous jump of w . The small- v_{ext} side of the plateau is difficult to address by numerical simulations, since the relative uncertainty in the determination of w increases due to v_{ext} -independent thermal fluctuations of $v_{\text{cm},x}(t)$. By running longer averaging simulations at low v_{ext} , we mitigate the error bars over w , and the data are consistent with a plateau dynamics extending all the way down to the static limit $v_{\text{ext}} \rightarrow 0$, like in the 1D model.⁸ In particular, within the plateau, the $T = 0$ calculation shows perfect matching of the mean lubricant velocity to the geometric ratio w_{plat} of Eq. (12). By increasing the temperature, w deviates more and more from the perfect plateau value. At the highest temperature considered, $k_B T = 0.5 \epsilon$, near melting of the LJ crystal at $k_B T_m \sim 0.7 \epsilon$,²⁰ and even at the smaller $k_B T = 0.25 \epsilon$ no strict plateau is observed in the simulations. Note however that for $v_{\text{ext}} \lesssim 0.5$ the plateau attractor tends to affect the dynamics even in the presence of large thermal fluctuations. We have checked that finite-size scaling shows essentially no size effect on the plateau, and in particular on its boundary edge v_{crit} .

The dynamical pinning mechanism of the present 2D model is similar to that discussed for the simpler 1D model.^{5,8} The bottom layer produces a corrugated potential energy which, with its near-matching periodicity, is responsible for the creation of kinks, generally consisting of weak local compressions of the lubricant chain, with two lubricant atoms trapped in the attractive region between two bottom-substrate atoms. In the quantized-velocity state, these kinks become pinned to the upper slider (whose potential varies slowly on the lubricant interparticle scale) and are therefore dragged along.

We probe the robustness of the quantized plateau state even in the presence of an “irregular” (i.e., quenched-disordered) bottom substrate, by running simulations with its atoms randomly displaced, horizontally and vertically, away from the regular positions, Eq. (5), by a significant fraction of the lattice equilibrium spacing a_b . Calculations still display the perfect plateau velocity, which however terminates at a lower v_{crit} . Figure 2b shows the results of one specific realization of the quenched disorder of 3 different amplitudes Σ . By averaging over different realizations of disorder with the same amplitude $\Sigma = 0.2 a_b$, we obtain, for example, $v_{\text{crit}} = 1.47 \pm 0.27$, compared to the value $v_{\text{crit}} \simeq 2.3$ obtained for the case a perfectly crystalline bottom wall at $T = 0$.

Our overall evidence is that, in the 2D system as much as in the more idealized 1D model, the phenomenon of

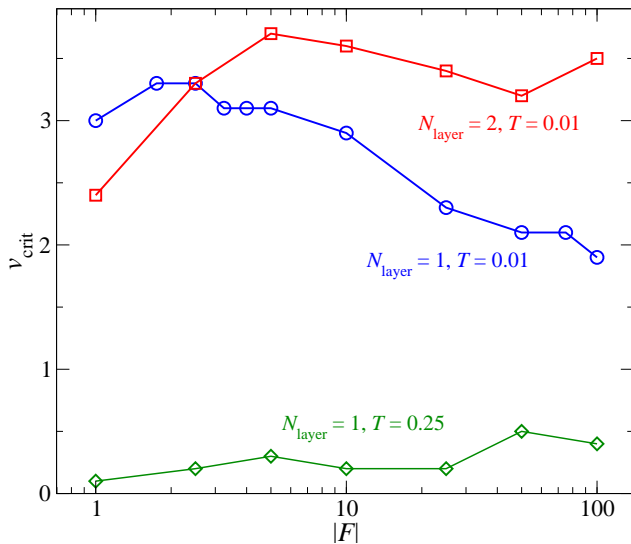


FIG. 3: (color online). The critical depinning velocity for the breakdown of the quantized plateau as a function of the applied load per top-layer atom F . For the 1-layer curves, the same geometry as in Fig. 2, temperatures $k_B T = 0.01$ (circles) and 0.25 (diamonds) are considered. The 2-layer curve (squares) is computed with a doubled number of lubricant atoms (58 rather than 29) confined between the same substrates in the same x -range.

velocity quantization is stable, reproducible and ubiquitous, and not the result of some careful tuning of parameters. In particular, Fig. 3 shows that the depinning velocity marking the end of the quantized plateau is a smooth function of the load F applied to the top layer over two orders of magnitude. Calculations suggest that a moderate load near unity is beneficial to the quantized sliding, at least at the low temperature $k_B T = 0.01\epsilon$. This is the result of a competition between the beneficial role of load that limits thermally induced “slips” of the kinks, and the detrimental effect of limiting the vertical lubricant movements at high loads. Indeed, at higher temperature, where thermal fluctuations are more active in destabilizing the quantized state (thus yielding a smaller v_{crit}), calculations show a general slow increase of v_{crit} with F , favored by the suppression of thermally induced “slips” promoted by the stronger load-induced confinement.

Figure 3 shows that in the large-load low-temperature regime, the critical velocity for $N_{\text{layer}} = 2$ is even larger than for $N_{\text{layer}} = 1$. In this plateau regime, we identify “horizontal” kinks in the lubricant layer adjacent to the bottom potential, while the upper lubricant layer shows weaker x -spacing modulations.

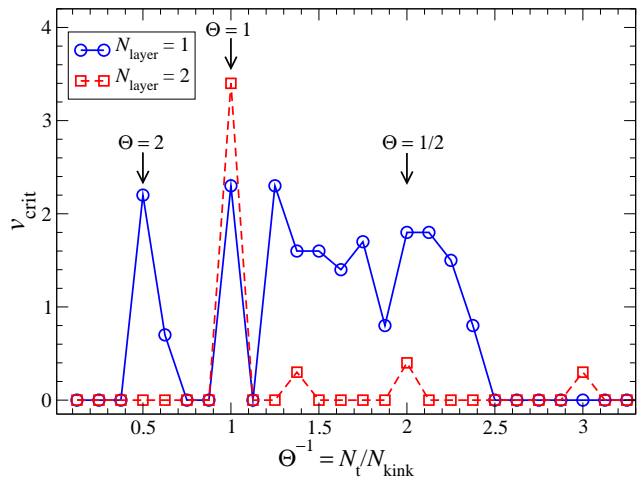


FIG. 4: (color online). Variation of the plateau boundary velocity v_{crit} as a function of the kink coverage $\Theta^{-1} = N_t/N_{\text{kink}}$ for a lubricant monolayer and bilayer. Calculations show local maxima of v_{crit} for commensurate values of Θ for both $N_{\text{layer}} = 1$ and 2; except at kink coverage $\Theta = 1$ v_{crit} is generally larger for $N_{\text{layer}} = 1$ than $N_{\text{layer}} = 2$. Simulations are carried out with $F = 25$, $T = 0.01$, and $\lambda_b = \frac{29}{25}$.

IV. SOLITON COVERAGE AND LUBRICANT SOFTNESS

The perfect matching of the number of kinks to the number of top-atoms $\Theta = N_{\text{kink}}/N_t = 1$, as considered in all previous figures, is an especially favorable circumstance for kink dragging, thus for the quantized-plateau phenomenon, but not one to be expected to occur easily in actual lubricated sliding. It is therefore important to examine situations where this kind of full commensuration is absent.

In the following we study the behavior of the depinning point v_{crit} as a function of the commensuration ratio Θ . In particular we keep λ_b fixed (i.e. the density of solitons), and vary the number of surface atoms in the top substrate. In Fig. 4 the depinning velocity v_{crit} , evaluated by adiabatically increasing of v_{ext} , is reported as a function of the commensuration ratio $\Theta^{-1} = N_t/N_{\text{kink}}$. While the dependence on kink coverage is rather erratic, we can recognize that v_{crit} tends to peak at or near integer values of Θ . In contrast, a fractional Θ displaced from commensurate regimes produces a weakening or even the loss of the quantized plateau, represented by $v_{\text{crit}} \simeq 0$. Figure 4 shows that this drop in v_{crit} is especially sharp for $N_{\text{layer}} = 2$, for which many incommensurate coverages show no quantized plateau, even at the smallest v_{ext} accessible within practical simulation times. We conclude that the occurrence of quantized lubricant velocity plateaus, although comparably robust and widespread, may not be trivial to observe in practice: strongly incommensurate coverages and/or thick lubricant films could prevent its manifestation.

The detailed dependence of the depinning transition

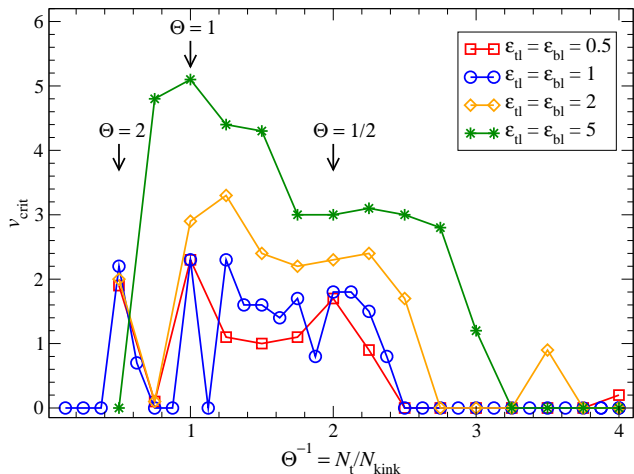


FIG. 5: (color online). Variation of the plateau boundary velocity v_{crit} as a function of the kink coverage $\Theta^{-1} = N_t/N_{\text{kink}}$ for a lubricant mono-layer showing different interaction energies with the substrates. Simulations are carried out with the same conditions as in Fig. 4, but with varied $\epsilon_{\text{tl}} = \epsilon_{\text{bl}}$, (but unchanged interparticle interaction $\epsilon_{\text{ll}} = \epsilon$).

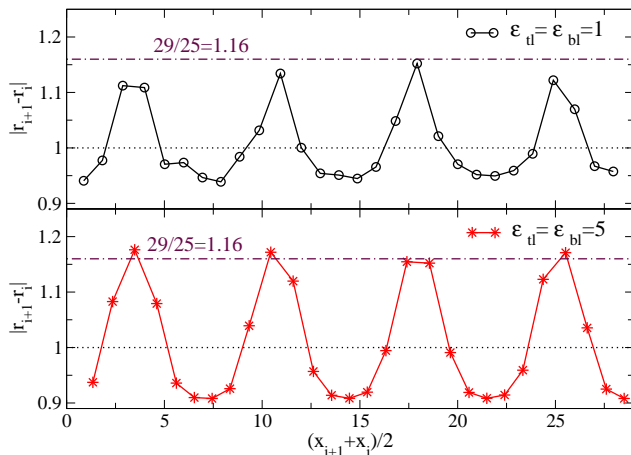


FIG. 6: (color online). Snapshot of the dynamically pinned state of the 2D lubricant, showing the bond lengths as a function of the bond horizontal position along the slider. Shorter bonds $\approx a_b$ identify kink regions, while longer bonds $\approx 1.16a_b$ belong to in-register regions. Larger interaction with the substrates $\epsilon_{\text{tl}} = \epsilon_{\text{bl}} > 1$ favors the commensurate in-register lubricant regions, shrinking the kink size.

on coverage is affected by the relative “softness” of the lubricant. Figure 5 shows that when the interaction energy $\epsilon_{\text{tl}} = \epsilon_{\text{bl}}$ of the lubricant with the substrates is increased to become larger than the intra-lubricant interaction ϵ_{ll} , as is the case for a soft lubricant wetting strongly the sliding surfaces, the quantized-plateau region extends generally to larger v_{ext} and to a wider range of coverages Θ . The reason for this is illustrated by the configuration snapshots of Fig. 6: a comparably stronger interaction with the substrates $\epsilon_{\text{tl}} = \epsilon_{\text{bl}} > 1$ favors the commensurate in-register lubricant regions, shrinking the kink size.

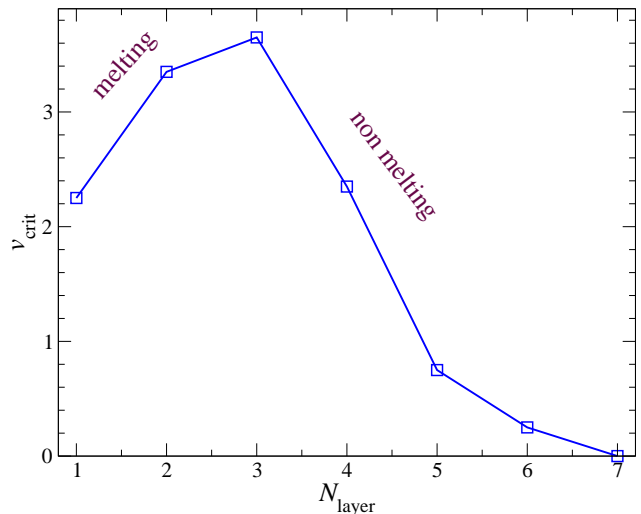


FIG. 7: (color online). Critical depinning velocity v_{crit} as a function of the numbers N_{layer} of lubricant layers. All simulations are carried out in a condition that favors the quantized-velocity sliding state: the model is composed by 4, $29 \cdot N_{\text{layer}}$ and 25 atoms in the top lubricant and bottom layers respectively (thus $\Theta = 1$), with an applied load $F = 25$ and $T = 0.01$. The data show an optimal dynamical pinning at $N_{\text{layer}} = 3$ and a tendency for v_{crit} to drop considerably as the lubricant thickness increases beyond that value. For $N_{\text{layer}} \geq 7$ no quantized plateau could be detected.

Localized kinks are more suitable to being picked up and dragged by the corrugations of the top substrate.

Figure 7 shows how the lubricant thickness affects the dynamically pinned state, i.e. v_{crit} as a function of the number N_{layer} of lubricant layers in the fully commensurate $\Theta = 1$ condition. The data show quantized-velocity plateaus, displaying a maximum extension for $N_{\text{layer}} = 3$, followed by a decaying v_{crit} as the lubricant thickness increases beyond that value. For $N_{\text{layer}} \geq 7$ layers we could detect no velocity plateau, at least within the v_{ext} range accessible to a practical numerical integration of the equations of motion. Vertical corrugations of the lubricant induced by the kinks originating and propagating from the bottom substrate have the effect of mediating the kink tendency to pin to the top-layer corrugations, therefore favoring the observed perfect velocity quantization. For increasing N_{layer} , these z -displacements decay rapidly, and this mechanism becomes less effective to support the dynamically pinned state.

Our calculations show that while the quantized plateau occurs when the solitons – misfit dislocations – are driven gently through the solid lubricant, the speed-induced transition to the $v_{\text{ext}} > v_{\text{crit}}$ dynamically unpinned state can involve the melting of the lubricant, due to the large Joule heating induced by shearing. By analyzing the detail of the depinning transition for $\Theta = 1$, we observe two different depinning behaviors to the left and to the right, respectively, of the maximum shown in Fig. 7. For $N_{\text{layer}} \leq 3$, the depinning transition changes the solid

lubricant film into a disordered diffusive liquid, with a lower density, (thus characterized by an increase in $\overline{r_{tz}}$). By contrast, a lubricant composed of four or more layers remains essentially solid through the depinning transition. This is the case because the Joule heating produced by shearing is removed with sufficient efficiency by the thermostat so that the effective lubricant temperature remains moderate. The lubricant remains solid in particular when v_{crit} is small, as is the case for thick lubricant layers, but also for $\Theta \neq 1$, or if a larger damping $\eta \simeq 1$ is introduced in the Langevin dynamics. This indicates that the quantitative details of the findings of the present section depend on the assumed dissipation mechanism, and could therefore vary between one or another specific experimental situation. Nonetheless the qualitative result that under suitable conditions the depinning could be associated to lubricant melting while under other conditions the lubricant could remain solid through the transition is expected to be real, and should be verifiable in real boundary-friction experiments.

V. FRICTION

The (x -directed) kinetic friction force F_k that must be applied to the top slider to maintain its sliding motion balances instantaneously the force that the lubricant exerts on the top substrate. F_k can be decomposed in several terms by analyzing the mechanical work done by the individual force contributions. The forces that the sliding top exerts on the lubricant [first term in Eq. (4)] produce a total work $W_{t \rightarrow 1}$ whose mean contribution to dissipation can be computed by evaluating the change in lubricant kinetic energy over a time interval Δt

$$\begin{aligned} E_k(t + \Delta t) - E_k(t) &= \quad (13) \\ &= \sum_j \int_t^{t+\Delta t} \left[\vec{F}_j + f_{\text{damp } j} + \vec{f}_j(t) \right] \cdot \dot{\vec{r}}_j dt' \\ &= \sum_j \int_t^{t+\Delta t} \vec{F}_j \cdot \dot{\vec{r}}_j dt' - \frac{4\eta}{m} \overline{E_k} \Delta t + \quad (14) \\ &+ \eta N_1 \int_t^{t+\Delta t} \vec{v}_{\text{cm}} \cdot \dot{\vec{r}}_t dt' + \sum_j \int_t^{t+\Delta t} \vec{f}_j \cdot \dot{\vec{r}}_j dt'. \end{aligned}$$

The first term in Eq. (14) represents precisely the contribution of the LJ top-lubricant interactions to $W_{t \rightarrow 1}$, plus bounded terms which do fluctuate, contributing a limited [order $O(\Delta t)^0$] potential-energy change in the limit of a long time integration. The second term is proportional to the kinetic energy averaged over the Δt time interval. The last term in (14) describes the correlation of the random forces and the lubricant velocities. By careful integration over the trajectory produced by the Langevin dynamics, averaging over the distribution of the random variables f_j (indicated by angular brackets), and recall-

ing Eq. (9), this term is evaluated as

$$\left\langle \int_t^{t+\Delta t} \vec{f}_j(t') \cdot \dot{\vec{r}}_j(t') dt' \right\rangle = \quad (15)$$

$$= \frac{1}{m} \int_t^{t+\Delta t} dt' \int_t^{t'} dt'' \langle \vec{f}_j(t') \cdot \vec{f}_j(t'') \rangle \quad (16)$$

$$= \frac{1}{m} \int_t^{t+\Delta t} dt' \int_t^{t'} dt'' 4\eta k_B T \delta(t' - t'') \times 2 \quad (17)$$

$$= \frac{8\eta k_B T}{m} \int_t^{t+\Delta t} dt' \frac{1}{2} = \frac{4\eta k_B T}{m} \Delta t. \quad (18)$$

The factor 2 in line (17) comes from summing \hat{x} and \hat{z} components, and the factor $\frac{1}{2}$ in the integral of line (18) is the result of integrating the Dirac delta at the integration boundary. We observe that, like the conservative potential energy terms, the lubricant kinetic energy deviation $E_k(t + \Delta t) - E_k(t)$ is of order $O(\Delta t)^0$ over a long time integration. By combining Eq. (14) with the result of Eq. (18), in this large- Δt limit the average dissipated work becomes

$$\begin{aligned} W_{t \rightarrow 1} &= \frac{4\eta}{m} \left[\overline{E_k} - N_1 k_B T - \frac{N_1}{4} m \overline{\vec{v}_{\text{cm}} \cdot \dot{\vec{r}}_t} \right. \quad (19) \\ &\quad \left. + \frac{N_1}{4} m \overline{(\dot{\vec{r}}_t - \vec{v}_{\text{cm}}) \cdot \dot{\vec{r}}_t} \right] \Delta t + O(\Delta t)^0. \quad (20) \end{aligned}$$

The fourth and last term in square brackets is added to account for the work done by the top substrate directly against the dissipation forces of Eq. (11). We omit the explicit indication of the averaging over the Langevin noise, which becomes irrelevant in the limit of a long averaging time Δt .

This total dissipated energy is conveniently written in a form where we measure the particles velocities relative to the instantaneous center-mass velocity \vec{v}_{cm} . Indeed, by using $\dot{\vec{r}}_i = (\dot{\vec{r}}_i - \vec{v}_{\text{cm}}) + \vec{v}_{\text{cm}}$ and omitting corrections of order $O(\Delta t^0)$, we can rewrite the dissipated energy as

$$\begin{aligned} W_{t \rightarrow 1} &= \frac{4\eta}{m} (\overline{E_{k \text{ cm}}} - N_1 k_B T) \Delta t \quad (21) \\ &+ \eta N_1 \left[\overline{v_{\text{cm}}^2} + \overline{(\dot{\vec{r}}_t - \vec{v}_{\text{cm}})^2} \right] \Delta t, \end{aligned}$$

where terms linear in $(\dot{\vec{r}}_i - \vec{v}_{\text{cm}})$ vanish due to the definition of \vec{v}_{cm} , and $E_{k \text{ cm}}$ is the kinetic energy in the instantaneous CM frame:

$$E_{k \text{ cm}} = \frac{m}{2} \sum_i (\dot{\vec{r}}_i - \vec{v}_{\text{cm}})^2. \quad (22)$$

The work that the top layer does on the lubricant is supplied by the kinetic friction force F_k [the top-substrate vertical motion only yields a work of order $O(\Delta t^0)$], and equals $F_k v_{\text{ext}} \Delta t$. This relation provides an instructive decomposition of the average kinetic friction force:

$$\begin{aligned} \overline{F_k} &= \frac{1}{v_{\text{ext}} \Delta t} W_{t \rightarrow 1} \quad (23) \\ &= \frac{4\eta}{m v_{\text{ext}}} (\overline{E_{k \text{ cm}}} - N_1 k_B T) \\ &\quad + \frac{\eta N_1}{v_{\text{ext}}} \left[\overline{v_{\text{cm}}^2} + \overline{(\dot{\vec{r}}_t - \vec{v}_{\text{cm}})^2} \right]. \end{aligned}$$

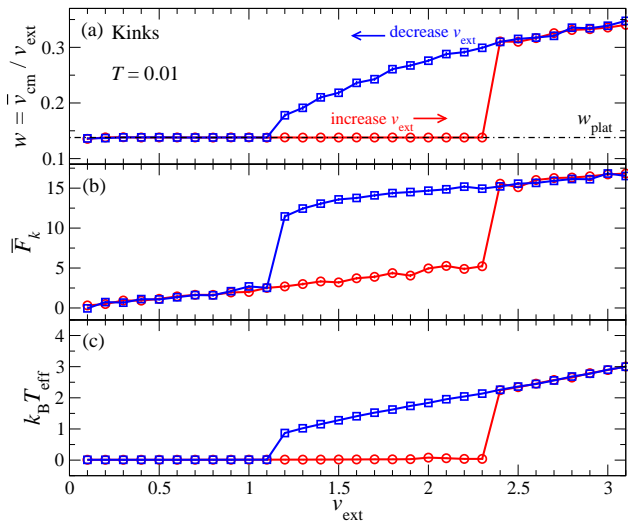


FIG. 8: (color online). Results of the same model as in Fig. 2 ($F = 25$, $T = 0.01$). As a function of the top-layer velocity v_{ext} adiabatically increased (circles) or decreased (squares) the three panels report: (a) the average velocity ratio $w = \overline{v_{\text{cm}x}}/v_{\text{ext}}$, compared to the plateau value $w_{\text{plat}} = \frac{4}{29} \simeq 0.138$, Eq. (12); (b) the average friction force experienced by the top layer; (c) the effective lubricant temperature, computed using the average kinetic energy in the frame of reference of the instantaneous lubricant center of mass, Eq. (24).

Equation (23) expresses the kinetic friction force \overline{F}_k as the sum of two contributions. The first and most important term is the contribution of the *fluctuations* of the lubricant-particle velocities in the instantaneous CM frame, reduced by the thermostat-set value. Even at $T = 0$, this term would vanish in the event that the lubricant moved as a rigid whole. The term in the final line can be interpreted as the friction force that dissipative phenomena with the bottom and the top respectively would produce, again even if the lubricant was rigid. This trivial term related to the overall CM motion yields a minimum total friction force whenever $\vec{v}_{\text{cm}} = \frac{1}{2} \dot{\vec{r}}_t$, which corresponds to $v_{\text{cm}x} = \frac{1}{2} v_{\text{ext}}$ for the main horizontal component. In fact, this trivial contribution originates the tendency of $w = \overline{v_{\text{cm}x}}/v_{\text{ext}}$ to abandon the plateau and reach 0.5, as in Figs. 2, and 8, 9 in the large sliding speed limit where this trivial term dominates. Equation (23) can be reformulated in terms of an effective temperature of the steady state:

$$\begin{aligned} k_{\text{B}} T_{\text{eff}} &= \frac{1}{N_1} \overline{E_{k\text{cm}}} \\ &= k_{\text{B}} T + \frac{m}{4} \left[\frac{v_{\text{ext}} \overline{F}_k}{\eta N_1} - \overline{v_{\text{cm}}^2} - \overline{(\dot{\vec{r}}_t - \vec{v}_{\text{cm}})^2} \right], \end{aligned} \quad (24)$$

The formulation (24), clarifies the contribution of friction to Joule heating, and shows explicitly the irrelevant role of the trivial dissipation terms in this respect.

Our MD simulations allow us to calculate instantaneously the (x -directed) kinetic friction by considering

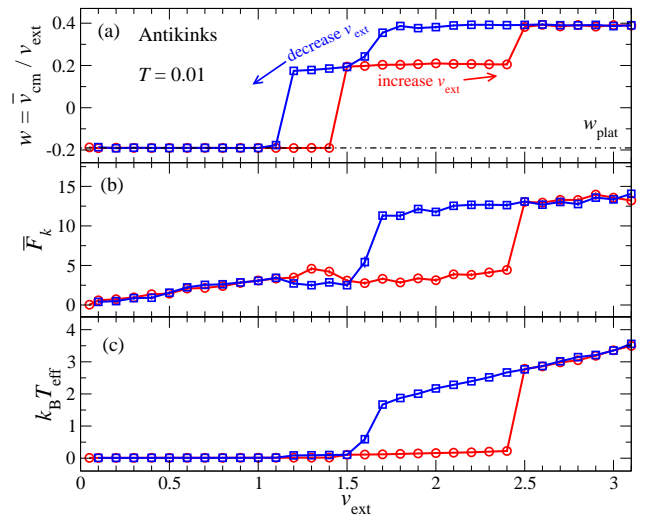


FIG. 9: (color online). Results of a model composed by 4, 21 and 25 atoms in the top, lubricant and bottom chains, $\lambda_b = 21/25 = 0.84$, which according to Eq. (12), produces perfectly quantized dynamics at a *negative* $w_{\text{plat}} = -\frac{4}{21} \simeq -0.190$, a dot-dashed line in panel a: this backward lubricant motion is caused by forward-dragged anti-kinks. The other simulation parameters are $F = 25$, $T = 0.01$. As a function of the top-layer velocity v_{ext} adiabatically increased (circles) or decreased (squares) the three panels report: (a) the average velocity ratio $w = \overline{v_{\text{cm}x}}/v_{\text{ext}}$; (b) the average friction force experienced by the top layer; (c) the effective lubricant temperature, Eq. (24).

the longitudinal force component that the lubricant exerts on the top driven substrate. By time averaging, the \overline{F}_k value obtained coincides precisely with that evaluated through Eq. (23).

A direct numerical evaluation of the friction force is shown in panels (b) of Figs. 8 and 9 for the kink and the anti-kink geometries, respectively, depicting typical scans where v_{ext} is cycled adiabatically up and down in small steps. Like in the $T = 0$ simulations of the 1D sliding model,^{7,8,12} and as is well known for the static pinning/depinning of the standard FK model,^{21–23} the present 2D model displays a clear hysteretic behavior of the velocity-plateau state (panels (a)), provided that thermal fluctuations are much smaller than the energy barrier hindering the full exploration of phase space for any affordable simulation time. A clear correlation of \overline{F}_k with the effective lubricant temperature $k_{\text{B}} T_{\text{eff}} \propto \overline{E_{k\text{cm}}}$ (panels Fig. 8c and 9c) is evident, but the trivial contribution is also seen to play a quantitative role. The bistability region with a clear hysteretic loop allows us to gauge the tribological effect of the quantized plateau state. In the kink geometry, Fig. 8 makes it apparent that friction is significantly less in the pinned quantized state than in the depinned state, all other parameters being equal. Figure 9 shows a similar tribological behavior, but with the occurrence of an additional intermediate approximately quantized velocity plateau (the 1D

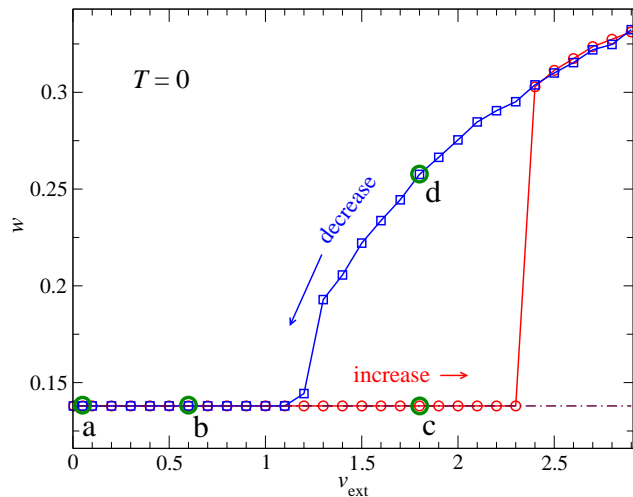


FIG. 10: (color online). The average velocity ratio $w = \overline{v_{\text{cm } x}}/v_{\text{ext}}$ as a function of the adiabatically increased (circles) or decreased (squares) top-layer velocity v_{ext} . The model parameters are the same as in Fig. 8, but with no thermal effects ($T = 0$).

model displayed similar intermediate plateaus⁵). The difference in friction between the primary and the secondary plateaus is a small one, with slightly less friction in the latter state. Comparison of the curves in panels 9b and 9c demonstrates that this effect is entirely due to the trivial friction term. This term is very large in the primary plateau because of the great difference of w from the optimal symmetrical drift $w = 0.5$; in passing to the secondary plateau, the trivial friction term decreases quite substantially, but the kinetic fluctuation contribution to friction increases by a similar amount.

VI. INTERMITTENT DYNAMICS AT THE PLATEAU STATE

So far, we assumed some fixed externally imposed speed for the top slider. In a standard tribological simulation, the slider is instead generally pulled through a spring of given stiffness whose other end is moved at constant velocity.²³ The spring can be viewed as a way to mimic not only the experimental driving device, but also the elasticity of the sliding substrates. From an experimental point of view, frictional forces may display a typical sawtooth dependence at sufficiently low driving external velocities, the hallmark of the intermittent stick-slip dynamics. The details of this low-driving behavior of course depend sensitively on the mechanical properties of the device that applies the stress.

Beside constant speed, we also explored the model with the spring pulling method. We obtained the quantized sliding state, also with the spring, and the simulations showed differences with the constant-speed method only in the fine detail. For this reason we omit here to display

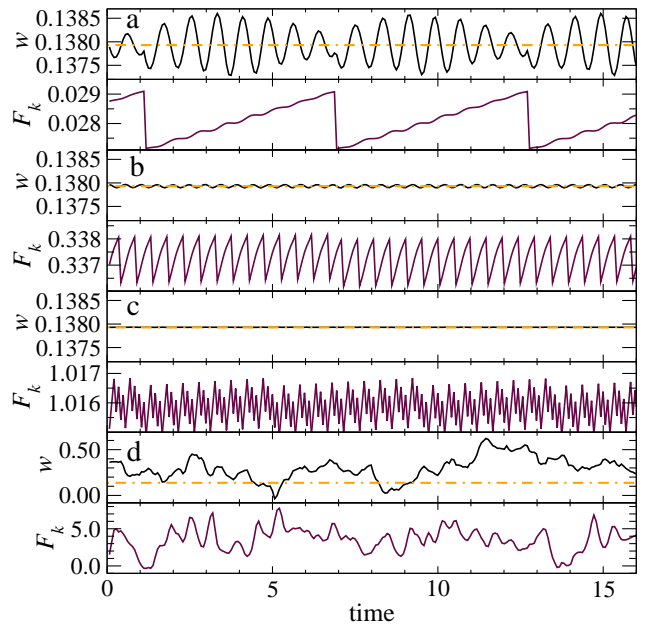


FIG. 11: (color online). The time evolution of the average velocity ratio w and the corresponding kinetic friction F_k for the four dynamical states (a), (b), (c), and (d) marked in Fig. 10. The first three panels, referring to quantized sliding states, display a typical intermittent stick-slip dynamics with small amplitude fluctuations; the last panel, not corresponding to a plateau state, exhibits chaotic large jumps in both w and F_k . The dot-dashed lines highlight the quantized-plateau value w_{plat} .

and analyze those results in detail.

In fact, even within the rigid-drive model, for sufficiently low sliding speed v_{ext} and for extremely small thermal fluctuations (i.e., $T \simeq 0$), we did observe a stick-slip intermittent dynamical regime in the total force applied to the sliding top substrate in order to keep its sliding speed constant. Figure 10 depicts a typical adiabatic up-down scan of v_{ext} , similar to Fig. 8a but at $T = 0$. To get insight into the different dynamical regimes outside and inside the bistability region, Fig. 11 analyzes in detail the four points marked in Fig. 10, three of which belong to the plateau state and one outside of it. Each of the four panels of Fig. 11 compares the time evolution of the lubricant CM velocity to the corresponding instantaneous kinetic friction force F_k .

For the first two plateau points (a) and (b) at low v_{ext} , the typical sawtooth time dependency of F_k is clearly visible. In these regimes of motion, the rescaled lubricant CM velocity $w = v_{\text{cm } x}/v_{\text{ext}}$ performs tiny periodic oscillations around the quantized plateau value and F_k exhibits an intermittent, almost regular, stick-slip pattern. This oscillatory phenomenology is understood as the kink array being dragged at full velocity v_{ext} across the associated periodic Peierls-Nabarro potential.²⁴ Indeed, the F_k oscillation frequency matches the washboard frequency of the kinks v_{ext}/a_b multiplied by their number $N_{\text{kink}} = N_t = 4$ in these $\Theta = 1$ simulations, due

to the four equally-spaced kinks crossing sequentially the corresponding Peierls-Nabarro barriers. A much less regular pattern would arise in a $\Theta \neq 1$ geometry. Due to the rather extended nature of solitons and smaller amplitude of the Peierls-Nabarro barrier with respect to the full atomic corrugation, the quantized plateau stick-slip regime is associated to much lower dissipation than regular stick-slip dynamics as seen in dry friction AFM experiments.^{25,26} By further increasing the external driving speed to $v_{\text{ext}} = 1.8$, panel (c), the kinetic friction becomes a little more “erratic”, with an extra modulation of the sawtooth shape, resembling a sort of inverted stick-slip. Panel (d) displays the dynamics for the same $v_{\text{ext}} = 1.8$, but obtained while cycling v_{ext} down: this depinned state shows large fluctuations both in w and F_k , giving rise to significant tribological dissipation, as expressed by the first term of Eq. (23).

VII. DISCUSSION AND CONCLUSIONS

The present simulation work is meant to characterize tribologically the quantized sliding state discovered in a 1D sliding model⁵ and later observed in a substantially less idealized 2D model.¹⁵ The perfectly quantized plateau is demonstrated here to extend over broad parameter ranges of the model, being robust against the effects of thermal fluctuations, quenched disorder in the confining substrates, the presence of confined multiple (up to 6) lubricant layers, and over a wide interval of loading forces. When temperature becomes comparable to the lubricant melting point, the plateau state tends to deteriorate and eventually disappears, but the geometrically determined velocity ratio w_{plat} , acting as an attractor, leaves anyway a trace in the ensuing “noisy” dynamics.

The velocity plateau, as a function of v_{ext} , ends at a critical velocity v_{crit} , and for $v_{\text{ext}} > v_{\text{crit}}$ the lubricant tends to accelerate toward a speed $0.5 v_{\text{ext}}$. This result, dictated by the symmetric choice of the Langevin thermostat dissipation, may change in real systems where heat dissipation occurs through generally asymmetric sliders.

Our calculations show that while the quantized plateau occurs when the solitons are driven gently through the solid lubricant, the speed-induced transition at $v_{\text{ext}} > v_{\text{crit}}$ can involve the melting of the lubricant, due to the large Joule heating induced by large velocity shearing. The depinning value v_{crit} is linked to the rate of commensuration Θ of kinks to the upper slider periodicity:

a particularly robust plateau signaled by a local maximum of v_{crit} is located at well-commensurate Θ values, especially $\Theta = 1$. Besides, the lubricant softness, setting the width of the propagating solitonic structures, is found to play a major role in promoting in-registry contact regions beneficial to this quantized sliding. Our typical dynamical depinning speed v_{crit} , is of the order of a few model units (corresponding to sliding speed values ranging from tens to thousands m/s for realistic choices of model parameters), is very large compared to typical sliding velocities investigated in experiments. This suggests that in practice sliding at a dynamically quantized velocity is likely to be extremely robust. In real experimental systems, deterioration of the quantized sliding state will most probably be associated to mechanisms such as disorder, boundary effects, or unfavorable lubricant-substrate incommensurate geometries, rather than to excessive driving speed.

By cycling v_{ext} in underdamped regime, the layer sliding velocity exhibits a hysteretic loop around v_{crit} , like in the 1D model.⁷ The bistability region allows us to gauge the tribological effect of the quantized plateau state. So, in the framework of Langevin dynamics, by evaluating the force instantaneously exerted on the top plate, we find that this quantized sliding represents a dynamical “pinned” state, characterized by significantly low values of the kinetic friction. A characteristic backward lubricant motion produced by the presence of “anti-kinks”, has also been observed in this context. This peculiar backward motion is likely to represent the most curious evidence of the quantized plateau state when – as we hope – it will be investigated experimentally.

On the theoretical side, the role of substrate deformability and defects in the lubricant structure, together with a realistic three dimensional description, with force fields representative of a concrete lubricated configurations, will certainly require further investigations.

Acknowledgments

This work was supported by CNR, as a part of the European Science Foundation EUROCORES Programme FANAS. R.C. and A.V. acknowledge gratefully the financial support by the Regional Laboratory InterMech - NetLab “Surfaces & Coatings for Advanced Mechanics and Nanomechanics” (SUP&RMAN), and of the European Commissions NEST Pathfinder program TRIGS under Contract No. NEST-2005-PATHCOM-043386.

¹ J. Gao, W. D. Luedtke, and U. Landman, *J. Chem. Phys.* **106**, 4309 (1997).

² U. Tartaglino, I. M. Sivebaek, B. N. J. Persson, and E. Tosatti, *J. Chem. Phys.* **125**, 014704 (2006).

³ J. Klein and E. Kumacheva, *J. Chem. Phys.* **108**, 6996 (1998).

⁴ G. He, M. H. Müser, Mark O. Robbins, *Science* **284**, 1650 (1999).

⁵ A. Vanossi, N. Manini, G. Divitini, G. E. Santoro, and E. Tosatti, *Phys. Rev. Lett.* **97**, 056101 (2006).

⁶ N. Manini, M. Cesaratto, G. E. Santoro, E. Tosatti, and A. Vanossi, *J. Phys.: Condens. Matter* **19**, 305016 (2007).

- ⁷ A. Vanossi, N. Manini, F. Caruso, G. E. Santoro, and E. Tosatti, Phys. Rev. Lett. **99**, 206101 (2007).
- ⁸ N. Manini, A. Vanossi, G. E. Santoro, and E. Tosatti, Phys. Rev. E **76**, 046603 (2007).
- ⁹ N. Manini, G. E. Santoro, E. Tosatti, and A. Vanossi, J. Phys.: Condens. Matter **20**, 224020 (2008).
- ¹⁰ G. E. Santoro, A. Vanossi, N. Manini, G. Divitini, and E. Tosatti, Surf. Sci. **600**, 2726 (2006).
- ¹¹ M. Cesaratto, N. Manini, A. Vanossi, E. Tosatti, and G. E. Santoro, Surf. Sci. **601**, 3682 (2007).
- ¹² A. Vanossi, G. E. Santoro, N. Manini, M. Cesaratto, and E. Tosatti, Surf. Sci. **601**, 3670 (2007).
- ¹³ A. Vanossi, G. E. Santoro, N. Manini, E. Tosatti, and O. M. Braun, Tribol. Int. **41**, 920 (2008).
- ¹⁴ O. M. Braun, A. Vanossi, and E. Tosatti, Phys. Rev. Lett. **95**, 026102 (2005).
- ¹⁵ I. E. Castelli, N. Manini, R. Capozza, A. Vanossi, G. E. Santoro, and E. Tosatti, J. Phys.: Condens. Matter **20**, 354005 (2008).
- ¹⁶ D. Frenkel and B. Smit, *Understanding Molecular Simulation. From Algorithms to Applications* (Academic Press, London, 1996).
- ¹⁷ G. J. Martyna, M. L. Klein and M. Tuckerman, J. Chem. Phys. **97**, 2635 (1992).
- ¹⁸ C. W. Gardiner, *Handbook of Stochastic Methods for Physics, Chemistry and the Natural Sciences* (Springer-Verlag, Berlin, 1985).
- ¹⁹ W. H. Press, S. A. Teukolsky, W. T. Vetterling and B. P. Flannery, *Numerical Recipes in Fortran. The Art of Parallel Scientific Computing* (Cambridge University Press, Cambridge, 1996).
- ²⁰ S. Ranganathan and K. N. Pathak, Phys. Rev. A **45**, 5789 (1992).
- ²¹ O. M. Braun, A. R. Bishop, and J. Röder, Phys. Rev. Lett. **79**, 3692 (1997).
- ²² A. Vanossi, G. Santoro, and V. Bortolani, J. Phys.: Condens. Matter **16**, S2895 (2004).
- ²³ A. Vanossi and O. M. Braun, J. Phys.: Condens. Matter **19**, 305017 (2007).
- ²⁴ O. M. Braun and Yu. S. Kivshar, *The Frenkel-Kontorova Model: Concepts, Methods, and Applications* (Springer-Verlag, Berlin, 2004).
- ²⁵ G. S. Verhoeven, M. Dienwiebel, and J. W. M. Frenken, Phys. Rev. B **70**, 165418 (2004).
- ²⁶ S. Maier, E. Gnecco, A. Baratoff, R. Bennewitz, and E. Meyer, Phys. Rev. B **78**, 045432 (2008).